SASEC2015
Third Southern African Solar Energy Conference
11 – 13 May 2015
Kruger National Park, South Africa

INSPECTING PV-PLANTS USING AERIAL, DRONE-MOUNTED INFRARED THERMOGRAPHY SYSTEM

Buerhop-Lutz Cl.* and Scheuerpflug H.
*Author for correspondence
Bavarian Center for Applied Energy Research,
ZAE Bayern,
91058 Erlangen,
Germany,
E-mail: claudia.buerhop-lutz@zae-bayern.de

ABSTRACT

Worldwide more than 140 GW photovoltaic plants are installed. The demand for testing methods for quality control of installed photovoltaic modules is increasing. Imaging techniques, like infrared imaging, are very popular. There are several advantages, providing two-dimensional images, measuring during operating conditions, fast and contactless as well as non-destructive. Mounting an infrared camera to a drone enhances the inspection but some specialties have to be considered. There are several factors influencing the image quality, as the observation angle, the flight altitude, the flight velocity which have to be chosen properly.

Besides the influence of the measurement parameters, IR-images of PV-plants and single modules will be shown. Depending on the temperature distribution evidence for specific failure modes are given. Thus, cell fracture, soldering failure, short-circuited cells, by-passed substrings, can be distinguished easily using IR-imaging. Further analyses verify the negative impact of the identified defects on the module performance.

INTRODUCTION

Worldwide more than 140 GW photovoltaic plants are installed [1]. 2013 more than 104.000.000 US-Dollars were invested. Thus, photovoltaic PV plays an increasing role for the global supply with electricity. Therefore safety and reliability aspects gain in importance for operation and maintenance of PV-plants. Monitoring, especially imaging techniques, like infrared (IR) thermography are valuable tools for inspecting PV-plants [2-6]. Recently, first results of electroluminescence imaging of installed PV-modules were published [7] providing more detail information of the modules but still is a time-consuming measurement from the ground. The mature technique is IR-imaging. Measurement systems consisting of an IR-camera and an aerial, unmanned vehicle visualize malfunctioning modules due to recorded temperature irregularities [8]. There are several benefits of this method: fast, reliable, non-destructive, contact-free and measuring during operating conditions. Furthermore, this technique is efficiently applicable to inaccessible roof mounted systems as well as to extended field plants, see the overview of a solar park in Figure 1.

For indoor investigations of PV-modules and solar cells many IR-based analysing techniques were developed successfully, e. g. [9]. Another helpful imaging technique for failure analysis of PV-modules is electroluminescence (EL) [10, 11]. Köntges [12], for example, used this technique to analyse the influence of micro-cracks in PV-modules on the power loss.

This paper focuses on two topics: first, fundamental aspects of IR-imaging relevant for inspecting PV-plants, second, the discussion of different failure modes and their impact on the performance of PV-modules and plants, including the their characteristics in IR-imaging.

Figure 1 Aerial Photograph of 3 MW solar park, optics with focal length 10 mm and aperture of 2.8

The impact of measurement parameters, e. g. observation angle [13], flight altitude [14], flight velocity, on the imaging quality, the measured temperature distribution, and the data evaluation will be presented in the fundamentals. In the results different failure modes will be dicussed. IR-images of PV-plants and single modules will be shown. Depending on the temperature distribution evidence for specific failure modes are given [15]. The influence of the series-connection on the modules is obvious and has been discussed elsewhere [16].

NOMENCLATURE

M	[W/m²]	Heat radiation
T	[°C]	Object temperature
ΔT	[K]	Temperature difference between hot spot and good neighbour cell
E	[W/m²]	Solar irradiation
P	[W]	Module power at mpp
Special characters		
σ	[W/m²/T⁴]	Boltzmann constant
ε	[-]	Emissivity coefficient
Subscripts		
amb		ambient
mpp		Maximum power point

Basics of temperature evaluation using IR-cameras for imaging installed PV-modules have been approached by other researchers [3]. The influence of the sky temperature has been discussed. The interaction of various effects like optical properties, flight parameters and local heat transfer phenomena, e. g. microclimate due to locally differing heat transfer and solar irradiation, with failure characteristics must be taken into account while analyzing installed PV-modules.

FUNDAMENTAL ASPECTS

Using infrared (IR) imaging visualizes heat radiation. The temperature can be calculated according to Stefan-Boltzmann-law. The heat radiation M emitted by a real body is determined by the Boltzmann constant ϭ, the emissivity ε and the body temperature T, according to

$$M = \sigma \cdot \epsilon \cdot T^4.$$

Since the emissivity of the heat source depends strongly on the material, its surface, the observation angle and the spectral region, these parameters have to be taken into account.

Besides the emissivity also the spatial resolution and motion blurring have to be considered using aerial IR-imaging of PV-plants, which will be discussed in the following paragraphs.

Observation angle

PV-modules typically are covered with a glass sheet. The emissivity of glass in the infrared spectral range is much higher than in the visible spectral range. It is highest at a perpendicular view ε ≈ 0,82 and reduces drastically with increasing angle, see Figure 2. Since the emissivity is much less than 1, significant amounts of reflected radiation from surrounding heat sources may influence the optical measurement, respectively, the IR-imaging of PV-plants.

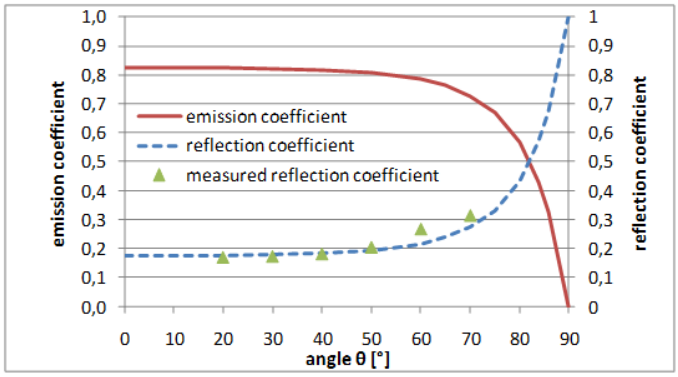

Figure 2 Measured reflectivity, respectively emissivity, of glass surface in the infrared spectral range from 8 to 10 µm [13]

Thus, different camera positions with respect to the module surface may result to differing observation angles, see Figure 3. Consequently, the emissivity of the heat radiation changes with the angular dependence. For camera position with flat view angles the emissivity of the modules differs strongly. For this example, the angle varies from 45° to 75° from one edge to the other. Even at a camera position in the middle of the stack the view angle increases up to 45° at the edges. Increasing the distance between IR-camera and modules the view angle decreases to 30°.

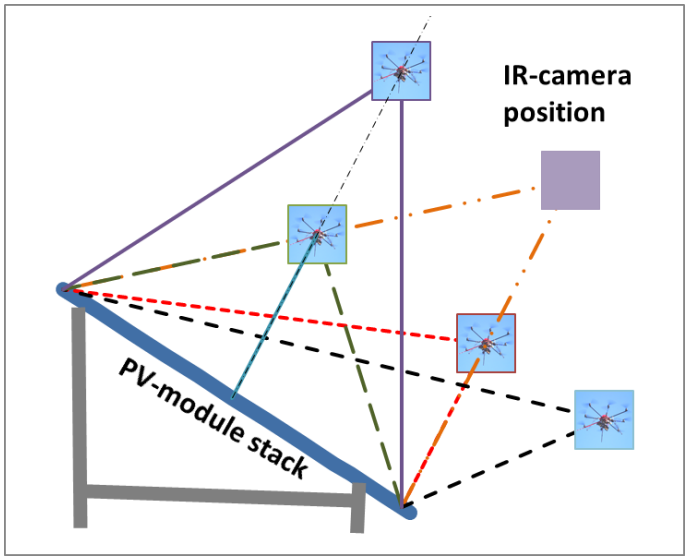

Figure 3 Schematic of different camera positions and the corresponding view angles for a module stack of about 11 m length and an inclination angle of 30°

How the different view angles and the resulting changes in emissivity may affect the temperature measurement is exemplarily shown in the following simulation. Therefore, the theoretically resulting object temperature is calculated using a simplified model [17] just considering the angular dependence

of the emissivity and reflectivity of the glass surface. The temperature of all modules was presumed to be at 39°C. The sky temperature (-2°C) as the reflecting object was taken into account, too.

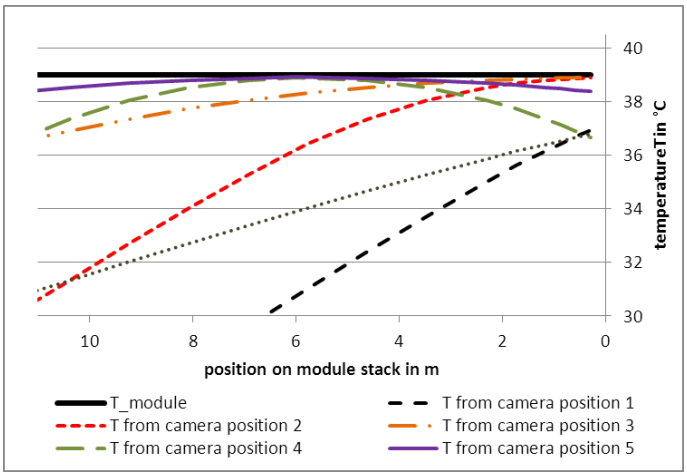

Figure 4 Calculated temperatures for an inclined module stack for different camera positions (camera positions correspond to the ones in Figure 3, same line styles).

The results are shown in Figure 4, the data correspond to the camera positions shown in Figure 3. For symmetric camera positions (4 and 5) with respect to the module stack, the emissivity stays fairly constant within the stack length because the change of view angle does not exceed 45°. Thus, the temperature is close to the real module temperature. The temperature deviation is within the measurement uncertainty. For the asymmetric camera positions (1, 2, and 3) the temperature drop on the left side (Figure 4) due to the large view angle is obvious. Here, the calculated temperature differs from the module temperature for more than 10 K easily. Thus, a not existing temperature gradient is suggested. This change of emissivity cannot be compensated by standard camera software.

This effect can be minimized if the view angle is close to perpendicular to the modules surface.

Lateral resolution

The lateral resolution is defined by the number of pixel per object which should be resolved, in this case, for example a solar cell or a solder joint. It is determined by the distance between the camera and the module surface. By increasing the distance the lateral resolution is reduced, the number of pixel per cell is reduced [14], [17]. The experiments yield that two cases can be distinguished: small heat sources with respect to the pixel size and extended heat sources. For extended heat sources the optically measured temperature only shows a minor dependence on the distance. It decreases slightly which is due to atmospheric absorption. In case of small heat sources a strong dependence of the temperature on the distance is observed. Figure 5 shows this behaviour of the measured temperature of a small and an extended heat source as a function of the lateral resolution. At high resolution (> 3 pixel/cell) the measured temperature is close to the real cell temperature. By decreasing the resolution (increasing the distance) the temperature drops continuously. At a resolution of about 1 pixel/cell it approaches the temperature of the surrounding neighbour cells. That means local heat sources, defects have the same temperature as their surrounding and are not visible anymore.

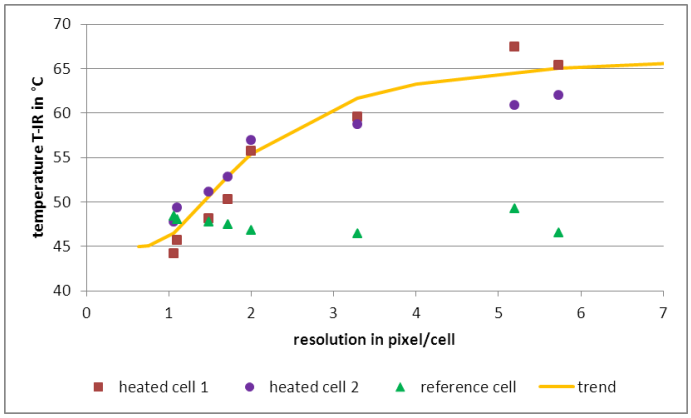

Figure 5 Optically measured temperature of small heat sources (heated solar cell 1 and 2) and extended areas (adjacent good cell acting as a reference cell) as a function of resolution [14]

Therefore, getting reliable temperature data using IR-cameras for inspecting PV-plants the resolution should be as high as possible.

Motion blurring

For inspecting PV-plants efficiently moving the IR-camera is essential. For high efficiency the inspection time should be as short as possible by a maximum of information and data reliability. Because of moving the camera motion blurring becomes important. It describes the sharpness of the object edges and therefore the ability to distinguish single, distinct features.

Motion blurring is influenced by the flight velocity and the resolution that means it depends on the flight height or distance. With increasing flight height the resolution reduces as explained above. With decreasing resolution the detected area by one pixel increases. Thus, the relative dislocation decreases. The lower the flight speed the smaller is the relative dislocation [17]. In detail motion blurring depends on the camera specification, its frame rate, and especially the used optics.

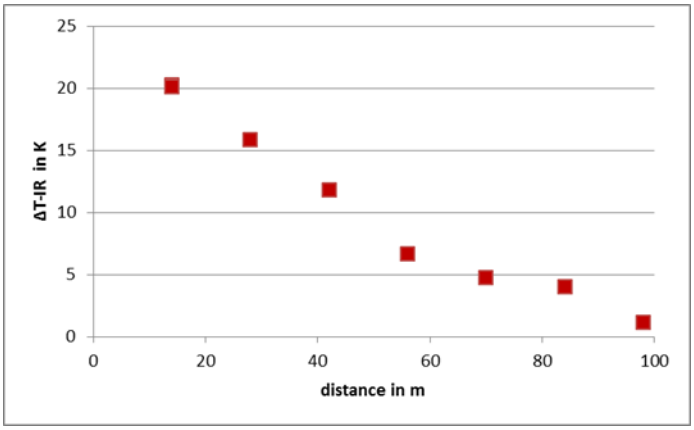

Figure 6 Temperature difference of the optically measured infrared temperatures of the hot defect cell and a regularly warmed good neighbour cell [14]

The previously described considerations have two contrary conclusions for the IR inspection of PV-plant using aerial drones: first, the distance to the panels should be rather short in order to realize a high lateral resolution and reliable temperatures, compare Figure 5. Figure 6 points out how the temperature difference, which is often taken as a measure of defect strength, decreases with increasing height. Second, the distance should be fairly large so that that motion blurring is minimized. Here, a compromise has to found.

EXPERIMENTAL PROCEDURE

For executing installed PV-modules or PV-plants aerial, drone mounted IR-imaging systems are used. The measurement system, as shown in Figure 7, consists of an unpiloted drone (Multikopter), a lightweight IR-camera PI 450 (Optris), a visible camera GoPro and equipment for navigating. The navigation system also allows the determination of the x, y, z-coordinates, so that the altitude of the camera is known. Using this setup the ideal perpendicular view on the modules can be easily realized and the crucial parameters, distance to the modules and flight velocity, adjusted properly.

Figure 7 Measurement system consisting of an octocopter carrying an IR bolometer and navigating equipment

In order to present frequently detected failure modes of installed PV-modules, typical examples from our aerial inspections of various PV-plants will be shown. The examples focus on crystalline modules from residential and industrial roofs as well as from solar parks in the field. The operating time reaches from fairly new installed plants up to several years of operating.

For analysing the failure mode all presented modules were dismounted and characterized further. Besides the outdoor aerial IR-imaging of the PV-plants, respectively the PV-modules connected in-series, indoor IR-imaging, electroluminescence imaging EL and IV-measurements were carried out. This enabled a better understanding of the module defects visualized in the IR-images in the field.

In Figure 8 and Figure 9 typical IR-images of roof-mounted PV-plants are shown miscoloured. The images depict the regular pattern of the mounted PV-modules (mostly yellow-green colour). In Figure 9 the metallic frame with two clamps at the lower and upper module edges (blue colour) is visible. The frame appears much colder than the glass surface of the modules due to the much lower emissivity of metals. For defect detection outstanding temperature irregularities are of interest, which will be discussed below.

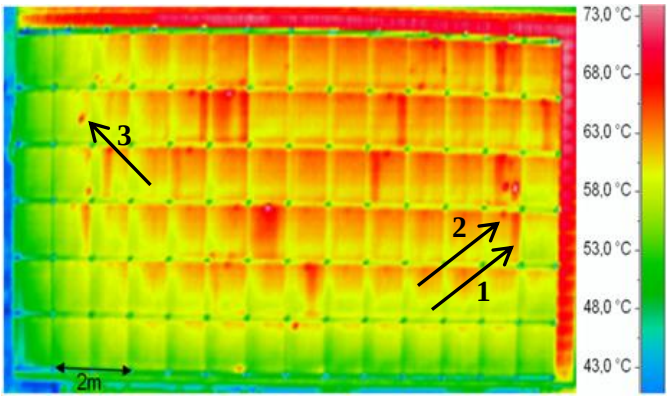

Figure 8 IR-images of a roof-mounted PV-plant 13,5 kW_p showing more PV-modules with outstanding locally risen temperature than unsuspicious ones, T_{amb} = 36°C, E = 900 W/m²

Concluding, for IR-inspections of PV-plants suitable and stable weather conditions are necessary. That means sufficient solar irradiation, no clouds (blue sky) and no wind for a certain period of time ensure analysable IR-images. If these requirements are fulfilled outstanding features indicate defect modules, which are localized easily using IR-imaging.

For the detail characterization the modules were dismounted and analysed in the lab. The IV-curves were measured using an AAA sun simulator SIM 4600 SLP (SPIRE). The EL-imaging was done with a Si-CCD camera coolSamBa HR-830 with 8.3 Mpixel (Sensovation). The format of the detector is 3326 x 2504 pixels. The modules are excited with an external power supply. The applied current was close to the short circuit current.

RESULTS – FAILURE MECHANISMS

IR-overviews of PV-plants (see fFigure 8 and Figure 9) provide a first impression of its quality. A homogeneous, regular temperature distribution indicates an equal quality of the modules. Periodically appearing features, like the upper module edge is warmer than the lower one, are due to convective heat transfer. These patterns can even be more outstanding across the entire PV-plant (see Figure 9). Singular appearing spots, cell, substrings or modules strings with elevated temperatures are a strong indication for faults. Since these faults lead to thermal loss, respectively local temperature rise, they are also linked with electric losses. In the following some modules defects and their impact on the module performance are described in detail.

Module string

There are entire module strings that have significantly increased temperatures compared to their neighbouring modules, compare Figure 9 (marked with an arrow). Typical temperature differences are 4 to 6 K. The homogeneous temperature distribution is a typical pattern for modules operating in open circuit. Solar radiation is absorbed and all the energy is converted to heat since no electric energy is generated. The most reasonable explanation is that this module string is not connected to the converter or the electric connection is lost. The electric power output is zero. The consequence is a significant power loss for such plant.

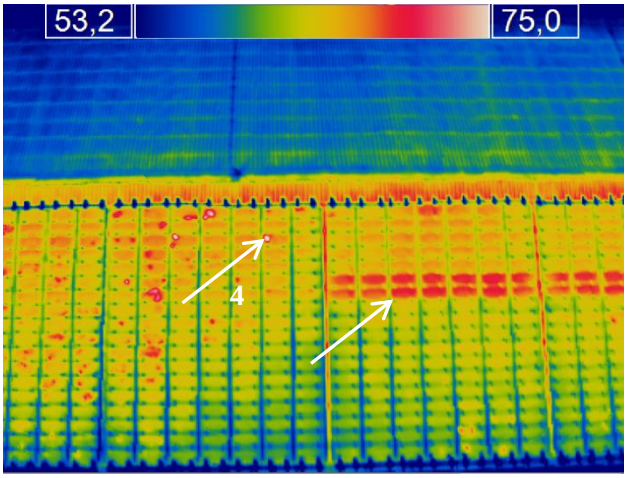

Figure 9 IR-image of a PV-plant section on an industrial roof 67 kW_p showing two entire module strings with elevated temperature in the right half, a large number of modules in the left half are suspicious, too, T_{amb} = 35°C, E = 1000 W/m²

Bypassed module substring

Bypassed module substrings are visible when module failures with a strong impact on the output power are present in PV-modules. In the PV-plant from Figure 8 several modules with bypassed substrings are visible, one example is marked with an arrow and number 1. Typical is that the cells of such a substring have a homogeneous, elevated temperature of about 4 to 6 K above the neighbouring cells and additionally that the corresponding bypass diode is operating and has a higher temperature (approx. 6 K) (marked with 2).

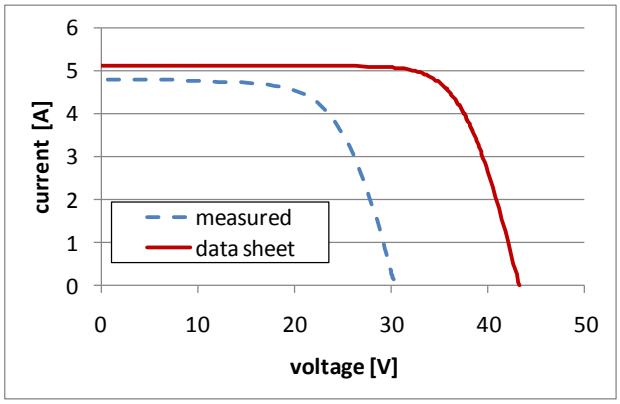

Figure 10 IV-curves of a PV-module with one bypassed substring, IV-curves: P (data sheet) = 165 W, P (bad module measured) = 95 W [15]

In case of one out of four substrings is bypassed by its bypass diode, the open circuit voltage is reduced by a quarter, compare Figure 10. The output power measured yields 95 W. More than a quarter of power is missing, which might be due to other defects in the un-bypassed substrings.

Cell fracture

Cell fracture is one of the most common faults in PV-modules. The origin can be manifold, manufacturing, transport, installation damage as well as natural degradation during life time. Fractured cells in PV-modules are visible in IR-images, see Figure 8 (marked with 3), because the cell parts heat up more strongly than the regular unbroken cells. The electrically unconnected fragments heat up because they operate in open circuit. The remaining connected parts have a smaller area so that the current density increases. Most important is the resulting current at the working point which is at the maximum power point (mpp) of the connected module string.

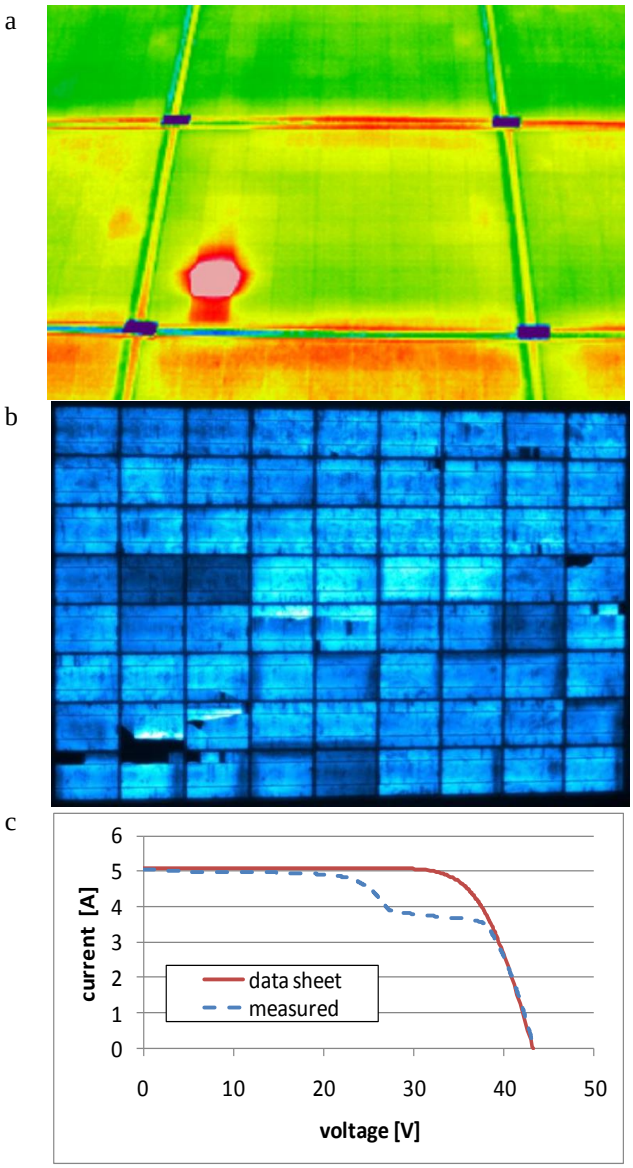

Figure 11 Detailed analysis of a module with cell fracture, a) IR-image at T_{amb} = 17°C, E = 650 W/m² and temperature difference at fractured solar cell ΔT = 40,6 K, b) EL-image and c) IV-curve: P (data sheet) = 165 W, P (bad module measured) = 133 W [15]

Figure 11 shows the IR-image and IV-curve of a module with cell fracture as can be seen in the EL-image. The cell with the strongest fracture has the highest temperature, here ΔT > 40 K. Small cell fractures, as seen in other cells of the same module, are of minor importance, no temperature increase is detected. Normally just the cell with the largest cell fracture shows the temperature increase. The temperature difference to the neighbour cells can be rather high depending on the fracture characteristics, the operating point, and the measurement conditions. (For example, we found sample module with ΔT > 100 K for distinct cells.) Therefore, the resulting module power is determined by the failure characteristics. This module has a power loss of 20% due to cell fracture at mpp.

Faulty soldering

Another frequent failure is the presence of faulty solderings. Typically, the temperature locally rises at the sites of open or bad solder joints, see Figure 9 (marked with 4). The area is much smaller than the area of a cell and will therefore is called hot spot. The IR-close-up in Figure 12 illustrates this exemplarily. Figure 12b shows the corresponding EL-image of the same module. At the outstanding sites of the IR-image a bright spot is stated in the EL-image presumably due to increased current density. The other features visible have no influence on the IR-image and apparently no impact on the module performance under operating conditions.

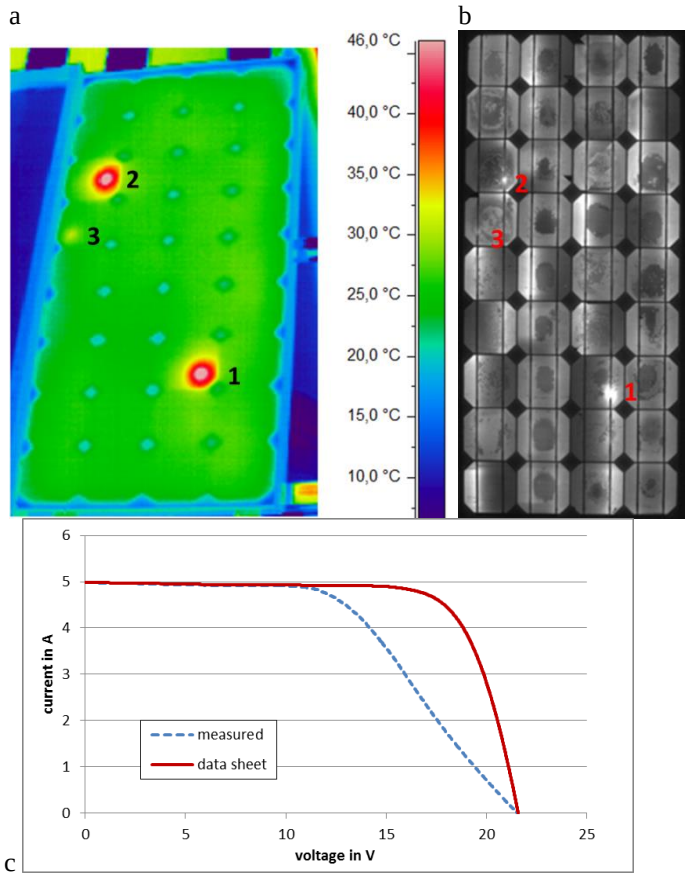

Figure 12 Detailed analysis of a module with bad solder joints, a) IR-image at T_{amb} = 12°C, E = 690 W/m² and temperature difference at bad solderings ΔT_1 = 26,3 K, ΔT_2 = 25,8 K, ΔT_3 = 4,2 K, b) EL-image, c) IV-curves: P (data sheet) = 80 W, P (bad module measured) = 57 W

Two spots show extremely high temperatures and a third one is still recognizable. There are temperature differences of ΔT > 25 K and ΔT > 4 K measurable. The number of such visible defects depends on the number of bad solder joints. The data evaluation yields that with increasing spot temperature the negative impact on the output power grows. Here, the output

power is almost reduced by 30% due to the increased series resistance, as seen in Figure 12c.

Shunted cell

Shunted cells result if front and back contacts of a solar cell are connected electrically. Then the current flows through the low-resistant contact and not passes the cell. Therefore, the affected solar cell is kind of short-circuited. Since the absorbed energy is not usable, the cell heats up. In Figure 13a these shunted cells have a slightly increased temperature, roughly $\Delta T > 1.5$ K. Several cells can be affected in one module. The corresponding EL-image (Figure 13b) depicts clearly, that through those cells no current flows. The cells appear darker or black. The influence on the output power is negligible for one shunted cell but for an increasing number of cells the output power can be decreased significantly. The power for the example module with 11 shunted cells is reduced by approximatley13%.

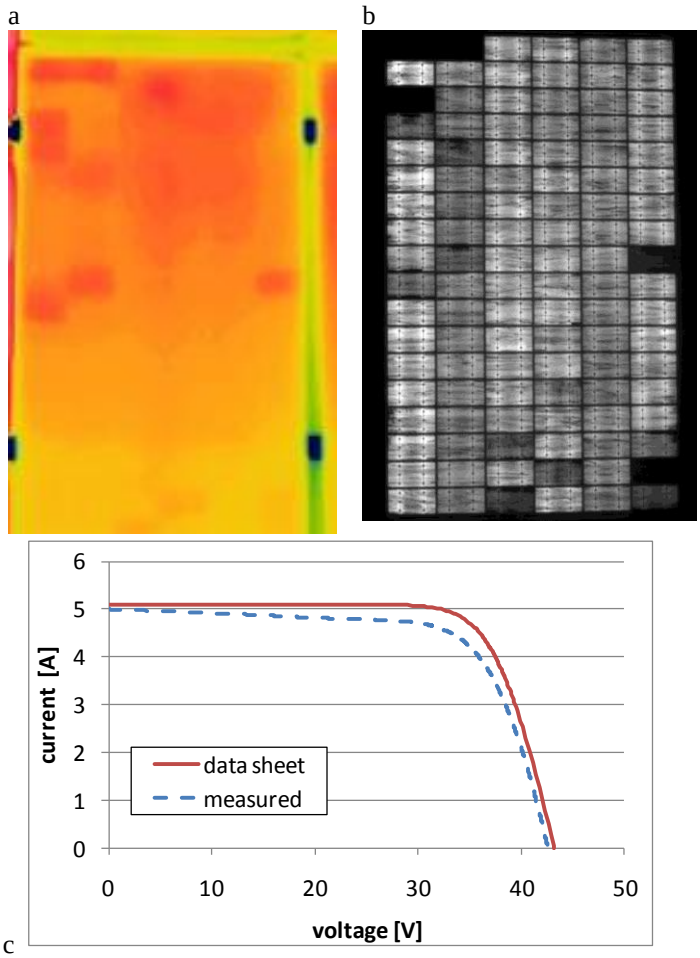

Figure 13 Detailed analysis of a module with shunted cells, a) IR-image at T_{amb} = 30°C, E = 850 W/m² and temperature difference at bad solderings ΔT = 2 K, b) EL-image, c) IV-curves: P (data sheet) = 190 W, P (bad module measured) = 165 W [15]

Defect bypass diode

Bypass diodes should prevent modules with defects from damage and excessive power loss. In case of strong failures, which can reduce the output power drastically and harm or even destroy the module, the bypass diode is active. Then, the current flows over the diode and the cells are bypassed, compare the section about bypassed substrings and Figure 8. If the bypass diode is stressed too much, it can be damaged, too. Supposed the diode becomes a good conducting resistor, the IV-curve changes, see Figure 14. The affected cell string works in short circuit, no output power is generated. The IR-image of such a string shows the typical patchwork pattern. If case of high conducting resistor or removal of the bypass diode the protection function of such a diode is lost, the output power is reduced strongly.

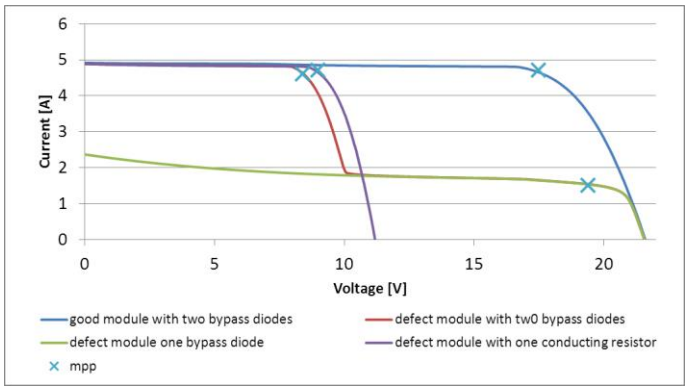

Figure 14: Measured IV-curves and mpp positions for different bypass diode situations of a test module: good module (P = 80 W, 2 bypass diodes), defect module (P = 38 W, 2 bypass diodes), defect module (P = 29 W, 1 bypass diode), defect module (P = 41 W, 1 bypass diode replaced by a good conducting resistor)

A typical IR-image of PV-module with a short-circuited bypass diode is seen in fFigure 15. One out of four substrings is affected by the defect bypass diode. In this example the lower substring shows the characteristic patchwork pattern of a short-circuited substring. Several cells are driven in reverse and therefore have an elevated temperature. The resulting temperatures depend on the IV-curves of the specific cells.

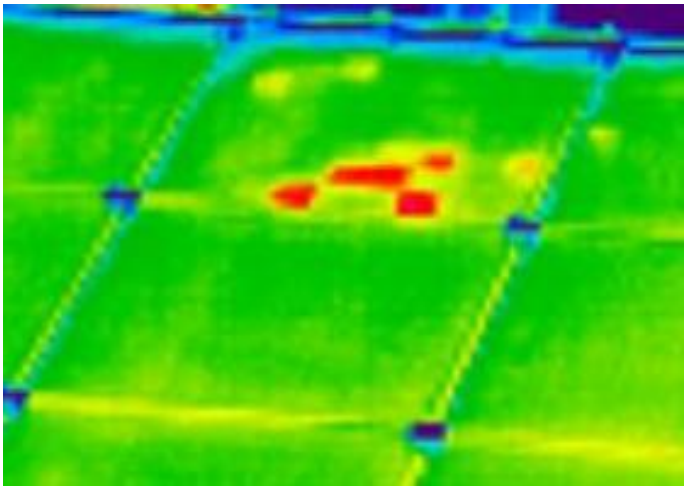

Figure 15: IR-image of a PV-module with a defect bypass diode showing several heated cells in the lower substring, (P (data sheet) = 165 W, 4 bypass diodes), defect module (P = 118 W, 3 bypass diodes intact, 1 bypass diode short-circuited)

Defect classification

Comparing the presented most common defects in PV-modules shows their specific characteristics in IR-images and power output. Table 1 gives a rough overview about the characteristics to distinguish different failure modes based on IR-images. In some cases, cell fracture, soldering and others, a specific temperature difference and power loss do not exist. Here, the values depend strongly on the distinct failure characteristics. Nevertheless, IR-inspections of PV-plants enhance a qualitative analysis of the module quality.

Table 1: Characteristics for different failure modes

	IR-image		IV-curve
	characteristic	ΔT [K]	P_{mpp} [W]
Module string	All cells hot	4 - 6	0
Substring	hot Substring cells	4 - 6	0 (for the substring)
Cell fracture	Mostly 1 hot cell	variable	variable
soldering	Several hot spots	variable	variable
Shunted cell	Several hot cells	1 - 1.5	variable
Bypass diode	Several cell at different temperature	variable	0 (for the substring)

SUMMARY

Aerial IR-inspecting systems are a valuable tool for qualitative analysis of PV-plants. If some requirements, like view angle, distance and flight velocity, are considered, a more quantitative data evaluation is enhanced and defects are distinguishable. A large number of different defects which influence the performance and power output can be visualized and localized. Bypassed substrings, cell fracture, bad solder joints, shunted cells, damaged bypass diodes can be distinguished by their characteristic appearance in IR-images.

REFERENCES

[1] EPIA, Global Market Outlook - For Photovoltaics 2014 - 2018, 2014, www.epia.org, last access: Sept. 29th, 2014

[2] Spagnolo G. S., Del Vecchio P., Makary G., Papalillo D., and Martocchia A., A review of IR thermography applied to PV systems, *Proceedings of the Environment and Electrical Engineering (EEEIC), 2012 11th International Conference on*, 2012, pp. 879-884

[3] Krenzinger A., and de Andrade A. C., Accurate outdoor glass thermographic thermometry applied to solar energy devices, *Solar Energy*, Vol. 81, 2007, pp. 1025-1034

[4] Buerhop C., Schlegel D., Niess M., and Vodermayer C., Quality Control of PV-Modules in the Field Using Infrared-Thermography, *Proceedings of the 26th PVSEC*, Hamburg, Germany, 2011, pp. 3894-3897

[5] King D. L., Kratochvil J. A., Quintana M. A., and McMahon T. J., Applications for infrared imaging equipment in photovoltaic cell, module, and system testing, *Proceedings of the Photovoltaic Specialists Conference, 2000. Conference Record of the Twenty-Eighth IEEE*, 2000, pp. 1487-1490

[6] Ancuta F., and Cepisca C., Fault analysis possibilities for PV panels, *Proceedings of the Proceedings of the 3rd International Youth Conference on Energetics (IYCE)*, 2011, pp. 1-5

[7] Stoicescu L., Reuter M., and Werner J. H., DaySy: Luminescence Imaging of PV-Modules in Daylight, *Proceedings of the 29th PVSEC*, Amsterdem, The Netherlands, 2014, pp. 2553-2554

[8] Buerhop C., Weißmann R., Scheuerpflug H., Auer R., and Brabec C. J., Quality control of PV-modules in the field using a remote-controlled drone with an infrared camera, *Proceedings of the 27th PVSEC*, Frankfurt, Germany, 2012, pp. 3370-3373

[9] Breitenstein O., Rakotoniaina J. P., and Al Rifai M. H., Quantitative evaluation of shunts in solar cells by lock-in thermography, *Progress in Photovoltaics*, Vol. 11, 2003, pp. 515-526

[10] Johnston S. W., Call N. J., Phan B., and Ahrenkiel R. K., Applications of imaging techniques for solar cell characterization, *Proceedings of the 34th IEEE, Photovoltaic Specialists Conference (PVSC)*, 2009, pp. 000276-000281

[11] Andor, Photovoltaic EL Imaging, http://www.andor.com/learning-academy/photovoltaic-el-imaging-an-overview-of-andor%27s-solutions-for-pv-el, last access: July 15th, 2013

[12] Köntges M., Kunze I., Kajari-Schröder S., Breitenmoser X., and Bjørneklett B., The risk of power loss in crystalline silicon based photovoltaic modules due to micro-cracks, *Solar Energy Materials and Solar Cells*, Vol. 95, 2011, pp. 1131-1137

[13] Buerhop C., Scheuerpflug H., and Weißmann R., The Role of Infrared Emissivity of Glass on IR-imaging of PV-Plants, *Proceedings of the 26th PVSEC*, Hamburg, Germany, 2011, pp. 3413-3416

[14] Buerhop C., and Scheuerpflug H., Field inspection of PV-modules using aerial, drone-mounted thermography, *Proceedings of the 29th PVSEC*, Amsterdem, The Netherlands, 2014, pp. 2975-2979

[15] Buerhop C., Schlegel D., Niess M., Vodermayer C., Weißmann R., and Brabec C. J., Reliability of IR-imaging of PV-plants under operating conditions, *Solar Energy Materials and Solar Cells*, Vol. 107, 2012, pp. 154-164

[16] Buerhop C., and Scheuerpflug H., Comparison of IR-Images and Module Performance under Standard and Field Conditions, *Proceedings of the 29th PVSEC*, Amsterdem, The Netherlands, 2014, pp. 3260-3264

[17] Buerhop C., and Scheuerpflug H., Radiometric study of installed PV using aerial thermogragphy, 2014, in preparation